J Mater Sci: Mater Electron (2021) 32:20891–20902

Facile synthesis of heterojunctions by hydrothermal decoration of CdS on electrospun $BiVO_4$ nanofibers with boosted photocatalytic activity

Long-Gui Peng[1], Fu-Rong Ni[1], Jun Liu[1,*], Meng Sun[1], Meng-Jie Chang[1], Tong Xi[1], Hui-Lu Li[1], Hui-Ling Du[1], Jie Yang[2], and Ying Li[1]

[1] College of Materials Science and Engineering, Xi'an University of Science and Technology, Xi'an 710054, China
[2] School of Safety Science and Engineering, Xi'an University of Science and Technology, Xi'an 710054, China

Received: 19 February 2021
Accepted: 24 June 2021
Published online: 14 July 2021

ABSTRACT

Bismuth vanadate ($BiVO_4$) is a promising photocatalyst material for photocatalytic degradation of organic pollutions. However, the fast recombination of photo-induced charge and insufficient light absorption often lead to poor photocatalytic performance. Herein, novel fibrous $BiVO_4$/CdS (BVO/CdS) heterostructures are constructed by uniformly modifying caterpillar shaped electrospun $BiVO_4$ nanofibers with controllable quantity of CdS nanoparticles through hydrothermal reaction. The absorption of visible light and separation efficiency of photo-generated charge of $BiVO_4$ are significantly promoted after the decoration of CdS nanoparticles. As a result, the photocatalytic efficiency of the optimized BVO/CdS sample (BVO/CdS-2 stands for the sample synthesized with 0.05 mmol $Cd(CH_3COO)_2$ and CH_4N_2S) is 90.43%, which is 3.3 times as high as that of pure $BiVO_4$ after 180 min irradiation under visible light, respectively. Moreover, the $.O_2^-$ and .OH are the predominant active species for the degradation process indicated by scavengers added photocatalytic experiments. Due to the simple, low-cost and controllable synthetic process, the BVO/CdS heterojunctions are suitable for practical usage.

1 Introduction

It is well known that environmental contamination has become one of the most urgent issues, especially the water pollution caused by various synthetic dyes. Photocatalytic technology based on nanostructured semiconductors has emerged as an effective and environmentally friendly strategy for the pollutant control [1, 2]. Titanium dioxide (TiO_2) has been used for the photodegradation of organic pollutants due to its low-cost, strong oxidizing ability and non-toxicity. Nevertheless, the bandgap of TiO_2 (3.2 eV) is relatively large and only a small fraction of sunlight can be utilized for photodegradation process. Thus, it remains the key point for designing semiconductor

Address correspondence to E-mail: jun_liu@xust.edu.cn

https://doi.org/10.1007/s10854-021-06605-y

photocatalysts that can harvest visible light of solar energy.

Bismuth vanadate ($BiVO_4$) has attracted great attentions for the characteristics of narrow bandgap energy, chemical stability and nontoxicity, which make $BiVO_4$ as a potential visible light photocatalyst for photocatalysis and photochemistry applications [3–5]. However, the photocatalytic activity of $BiVO_4$ alone is severely hampered by the fast recombination rate and low separation efficiency of photo-induced charge carries, which significantly limit the practical needs. To satisfy the photocatalytic usage of $BiVO_4$, more effective heterojunctions by coupling two different semiconductors were developed to assist charge separation and increase lifetime of photogenerated electron–hole pairs. To date, a variety of nanostructure materials have been integrated with $BiVO_4$ to achieve high photocatalytic activity [6–14]. As a typical transition metal sulfide, cadmium sulfide (CdS) is appropriate to be an excellent photoactive material in pollutant degradation, hydrogen production and solar cells due to the advantages of narrow bandgap (2.4 eV) and high absorption coefficient [15–18]. Meanwhile, the CdS has proper band position to couple with $BiVO_4$ to form heterojunctions. Therefore, CdS featured with special bandgap structure and strong visible light absorption has been utilized to construct $BiVO_4$/CdS (BVO/CdS) photocatalyst to achieve an ideal photocatalytic activity [19–29]. In spite of this, it should be noted that the powder shaped $BiVO_4$/CdS samples generally fabricated by hydrothermal and subsequent photodeposition or electrostatic adsorption procedures might suffer from several shortcomings such as hard separation from solution, easy to aggregation and possible secondary pollution.

In contrast with other synthetic approaches, electrospinning method has been extensively explored for producing one-dimensional nanofabric materials with various compositions and controllable morphologies, which provide promising application in electrochemistry and photocatalysis. The electrospun fibers present excellent photocatalytic performance owing to their merit of high surface-to- volume ratios [30, 31]. Moreover, nanofibers can serve as suitable supports to avoid the aggregation of nanosized interfacial contact when building heterojunction with other materials. Taking advantages of such method, $BiVO_4$ with various morphologies such as porous [32], nanobelt [33], solid [34], nanotube [35], bamboo [36], etc., have been prepared via electrospinning. In order to further boost the photocatalytic activity, Ag/C [37] and Mo [38] composited with $BiVO_4$ nanofibers were successfully fabricated. Therefore, construction of one-dimensional $BiVO_4$/CdS heterojunctions should be greatly desired for the photocatalysis application. Motivated by the above concerns, herein we report a successful attempt for the preparation of $BiVO_4$/CdS heterojunctions by hydrothermal growth of CdS nanoparticles on electrospun $BiVO_4$ nanofibers for dye degradation. The quantities of loaded CdS on the photocatalytic performance was investigated, and the possible photocatalytic mechanism were proposed.

2 Experimental

2.1 Materials

Bismuth nitrate pentahydrate ($Bi(NO_3)_3{\cdot}5H_2O$), cadmium acetate dihydrate ($Cd(CH_3COO)_2{\cdot}2H_2O$), thiourea ($CH_4N_2S$) and organic solvents were purchased from Guoyao Chemical Co., China. Polyvinylpyrrolidone (PVP, Mw = 1,300,000 g mol^{-1}) and vanadyl acetylacetonate ($VO(acac)_2$) were acquired from Aladdin Inc. All regents used in this work are of analytical grade without any further purification.

2.2 Fabrication of electrospun $BiVO_4$ nanofibers

$BiVO_4$ nanofibers were fabricated by electrospun method (Fig. 1a, b). In a typical procedure, 1.21 g of $Bi(NO_3)_3{\cdot}5H_2O$, 0.7 g of PVP and 0.662 g of $VO(acac)_2$ were dissolved into a mixed solvent containing 1.9 mL of acetic acid, 3.2 mL of ethanol and 2.6 mL of N,N-dimethylformamide. After being stirred for at least 6 h at room temperature, the above homogeneous green precursor solution was loaded into a 1 mL syringe for electrospinning. The solution was extruded out at a feeding rate of 8 μL min^{-1} under a voltage potential of 9 kV with a fixed distance of 15 cm between the two electrodes. The collected as-spun nanofibers from negatively charged foil were calcined at a rate of 5 °C min^{-1} up to 500 °C for 2 h in air to produce electrospun $BiVO_4$ nanofibers.

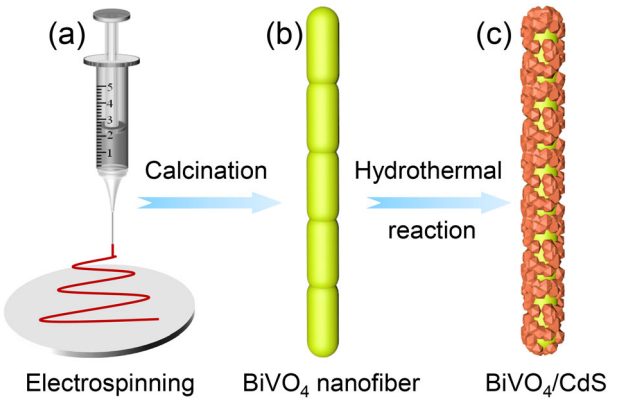

Fig. 1 Scheme for fabricating BVO/CdS heterojunctions: electrospinning and calcination to form $BiVO_4$ nanofibers (**a**, **b**); hydrothermal deposition of CdS nanoparticles (**c**)

2.3 Preparation of $BiVO_4$/CdS heterojunctions by hydrothermal method

The $BiVO_4$/CdS composites were prepared by hydrothermal method (Fig. 1c). First, the precursor solution was prepared by mixing 15 mL of $Cd(CH_3COO)_2$ solution with 15 mL of CH_4N_2S aqueous solution with equal concentration. Then the above solution together with 30 mg of $BiVO_4$ fiber was transferred into a 50 mL Teflon-lined autoclave and was maintained at 90 °C for 12 h in an electric oven. After washed with deionized water for three times, the products were dried at 70 °C for 6 h. The samples synthesized with $Cd(CH_3COO)_2$ of 0.025, 0.05 and 0.1 mmol were simplified as BVO/CdS-1, BVO/CdS-2 and BVO/CdS-3, respectively. The same concentration of CH_4N_2S with $Cd(CH_3COO)_2$ was used for the synthesis of each sample.

2.4 Characterization

Scanning electron microscopy (SEM) images were captured with a Hitachi S-4800 microscope at an accelerated voltage of 5 kV. Samples were directly adhered on conductive tape substrate and deposited with a thin layer of gold before SEM measurement. Transmission electron microscopy (TEM) and high-resolution transmission electron microscopy (HRTEM) were performed using a JEM-2100 microscope at an accelerated voltage of 300 kV. The TEM samples were prepared by evaporating a drop of aqueous product on a lacey carbon-copper TEM grid. Phase composition and crystal structure were measured with powder X-ray diffraction (XRD) method (Shimadzu D6000) with Cu Ka radiation at a scan rate of 0.02° per step. The ultraviolet–visible diffuse reflectance (UV–vis DR) spectra were recorded using a Shimadzu UV-2600 spectrometer by using $BaSO_4$ as a reference. X-ray photoelectron spectroscopy (XPS) was detected with a PHI-5702 X-ray photoelectron spectrometer. The photoelectrochemical measurements were performed on an electrochemical workstation (CHI 660E, Chenhua, Shanghai). In the conventional three-electrode system, a Pt foil and Ag/AgCl (saturated KCl) were used as counter and reference electrode, respectively. Fluorine doped tin oxide (FTO) glass covered with 1 cm^2 of ethanol slurry including 0.2 mg of prepared samples was used as work electrode. The photocurrents were measured in 0.1 M Na_2SO_4 electrolyte.

The photocatalytic performance of the products was evaluated by photodegradation of RhB solution in air. Typically, 10 mg of the catalyst was added into 10 mL RhB (10 mg L^{-1}) solution and the solution was kept for 30 min in dark to reach adsorption–desorption equilibrium. Then the photodegradation experiment was conducted under visible light irradiation using a Xe lamp (PLS-SEX 300UV) with a 400 nm UV cut-off filter without stirring. The centrifuged solution was analyzed at given 30 min intervals using a T6 UV–vis spectrophotometer. The maximum absorption at 554 nm of RhB was used to calculate the degraded efficiency. A radical trapping experiment was carried out in the presence of scavengers of ethylenediaminetetraacetic acid disodium (EDTA-2Na, 0.5 mM), 4-benzoquinone (BQ, 0.01 mM) and isopropanol (IPA, 1 mM), respectively. In this work, all the BVO/CdS-1, BVO/CdS-2 and BVO/CdS-3 samples display better photocatalyltic activity than that of pure $BiVO_4$ nanofibers, and the BVO/CdS-2 has the best photocatalytic performance. Therefore, the TEM, XPS, UV–vis DR and N_2 adsorption–desorption isotherms characterization were conducted only for the BVO/CdS-2 sample.

3 Results and discussion

3.1 Composition and microstructure of $BiVO_4$/CdS nanofibers

The crystallographic structure of $BiVO_4$ and BVO/CdS composites were examined by XRD. As

illustrated in Fig. 2a, the XRD pattern of $BiVO_4$ nanofibers shows peaks at 28.95°, 30.56°, 34.52°, 35.36°, 39.84°, 42.48°, 46.74°, 47.43°, 53.38°, 58.53° and 59.46°, corresponding to the (112), (004), (200), (020), (211), (015), (204), (024), (116), (312) and (132) crystal planes of monoclinic phase $BiVO_4$ (JCPDS 15-2480) [39], respectively. In the case of BVO/CdS-3 (Fig. 2d), except for characteristic peaks of $BiVO_4$, another two diffraction peaks centered at 24.82° and 28.22° can be indexed to (002) and (101) planes of hexagonal CdS (JCPDS 41-1049) [40], indicating that BVO/CdS-3 nanofiber is made up of $BiVO_4$ and hexagonal CdS. Due to the relatively low quantity of CdS nanoparticles, the peaks of CdS in BVO/CdS-1 and BVO/CdS-2 samples are not as strong as that in the BVO/CdS-3 sample (Fig. 2b and c).

The SEM and TEM images illustrating the morphology of as-prepared samples are presented in Fig. 3. It is clear that the obtained $BiVO_4$ nanofibers possess caterpillar fibrous shape with smooth surface of around 200 nm in diameter (Fig. 3a). Some nanoparticles can be observed uniformly distributed on the fiber surface after the hydrothermal process, indicating the formation of CdS nanoparticles. Particularly, only partial $BiVO_4$ surface are coated by CdS nanoparticles for BVO/CdS-1 and BVO/CdS-2 samples due to relatively small amounts of resulted CdS nanoparticles. In contrast, the whole surface of the $BiVO_4$ is encapsulated with dense CdS nanoparticles with continuously increasing the concentration of CdS precursor for BVO/CdS-3, suggesting that the quantity of loaded CdS nanoparticles can be easily

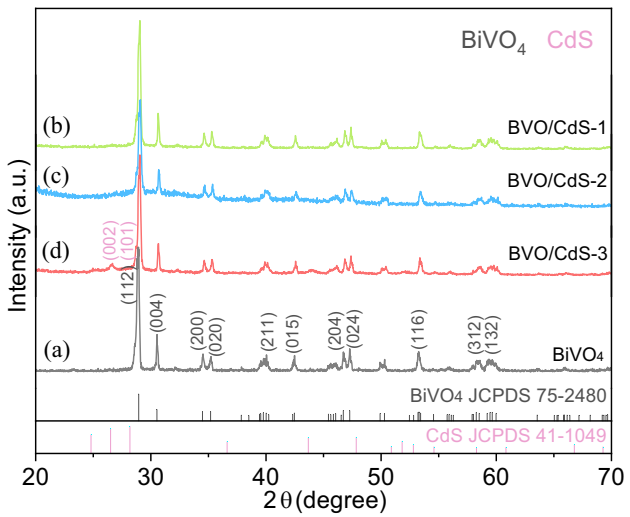

Fig. 2 XRD plots of $BiVO_4$ (a) and BVO/CdS composites (b–d)

controlled by the precursor concentrations. The core/shell structure of BVO/CdS-2 nanofibers was further investigated by TEM and HRTEM images. In Fig. 3e, the $BiVO_4$ fibers display deep color inside and CdS nanoparticles exhibit light color outside. The CdS nanoparticles presents unregular morphology with a dimeter of about 40 nm, which is much larger than that synthesized with by electrostatic interaction (~ 20 nm). The lattice distance of 0.475 and 0.357 nm agree well with (101) plane of $BiVO_4$ and (100) facet of CdS, respectively. Meanwhile, the CdS and $BiVO_4$ have intact interface, which is important for the charge transfer and enhancement of photocatalytic activity. These observations reveal that CdS nanoparticles with high crystalline are successfully generated during hydrothermal process and BVO/CdS nanofibers were acquired.

Figure 4a exhibits the energy dispersive spectroscopy (EDS) results of BVO/CdS-2 nanofibers. It reveals that five elements including O, S, Bi, Cd and V are co-existed in the resultant BVO/CdS-2 nanofibers. Meanwhile, the atom and weight ratios of different atoms are constant with the composition of $BiVO_4$ and CdS, indicating that the CdS has a weight ratio approximate 10.36% in the BVO/CdS-2 hybrid nanofibers. The elemental mapping images of Bi, V and O display even distribution throughout the entire fiber (Fig. 4c–e). Moreover, signals from Cd and S elements demonstrate that CdS nanoparticles are homogeneously and densely grown on each $BiVO_4$ fiber body (Fig. 4f–g). Thus, the above results further confirm the successful immobilization of CdS nanoparticles on $BiVO_4$ fiber surface, which is agreed with TEM analysis.

XPS analysis was performed to characterize the surface chemical compositions of BVO/CdS-2 nanofibers. In consistent with elemental mappings of BVO/CdS-2, the survey spectrum confirms the existence of Bi, S, Cd, V and O elements in the hybrid fiber (Fig. 5a). The high-resolution Bi 4f spectrum (Fig. 5b) can be fitted to two peaks located at 158.5 and 163.6 eV corresponding to Bi $4f_{7/2}$ and Bi $4f_{5/2}$ of Bi^{3+} [41], respectively, while the peaks at around 161.2 eV belongs the presence of S^{2-}. The peak centered at binding energy of 530.6 eV in the O 1 s spectrum reveals the existence of V–O in BVO/CdS-2 nanofibers, and the peak at 532.9 eV can be assigned to the surface adsorbed oxygen specie (Fig. 5c). For V 2p in Fig. 5d, a pair of peaks at about 517.3 and 524.9 eV are attributed to V $2p_{3/2}$ and V $2p_{1/2}$

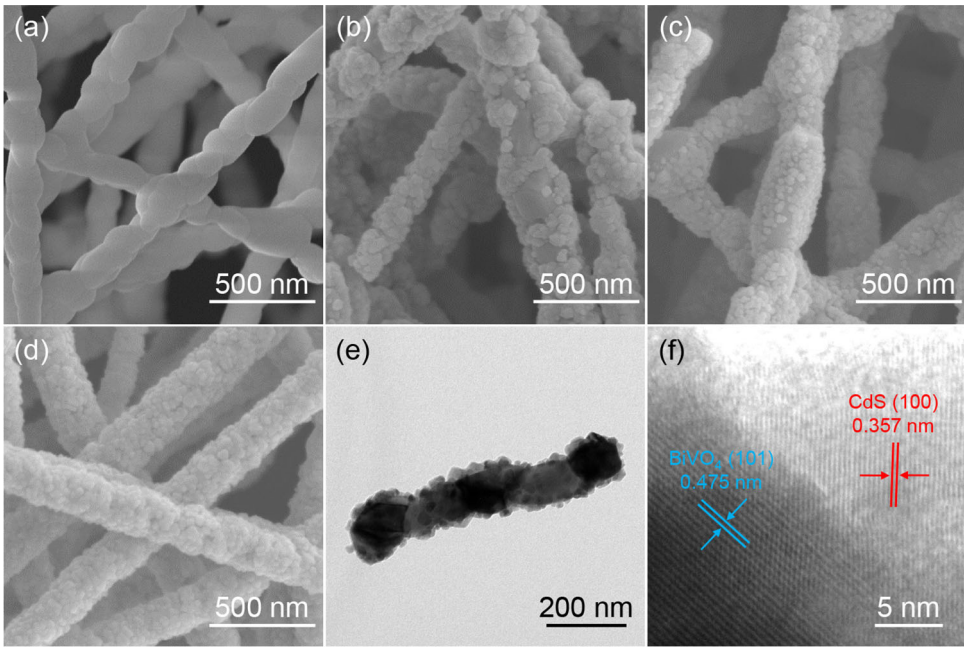

Fig. 3 SEM images of $BiVO_4$ (**a**) and BVO/CdS composites (**b**–**d**); TEM and HRTEM images of BVO/CdS-2 (**e**, **f**)

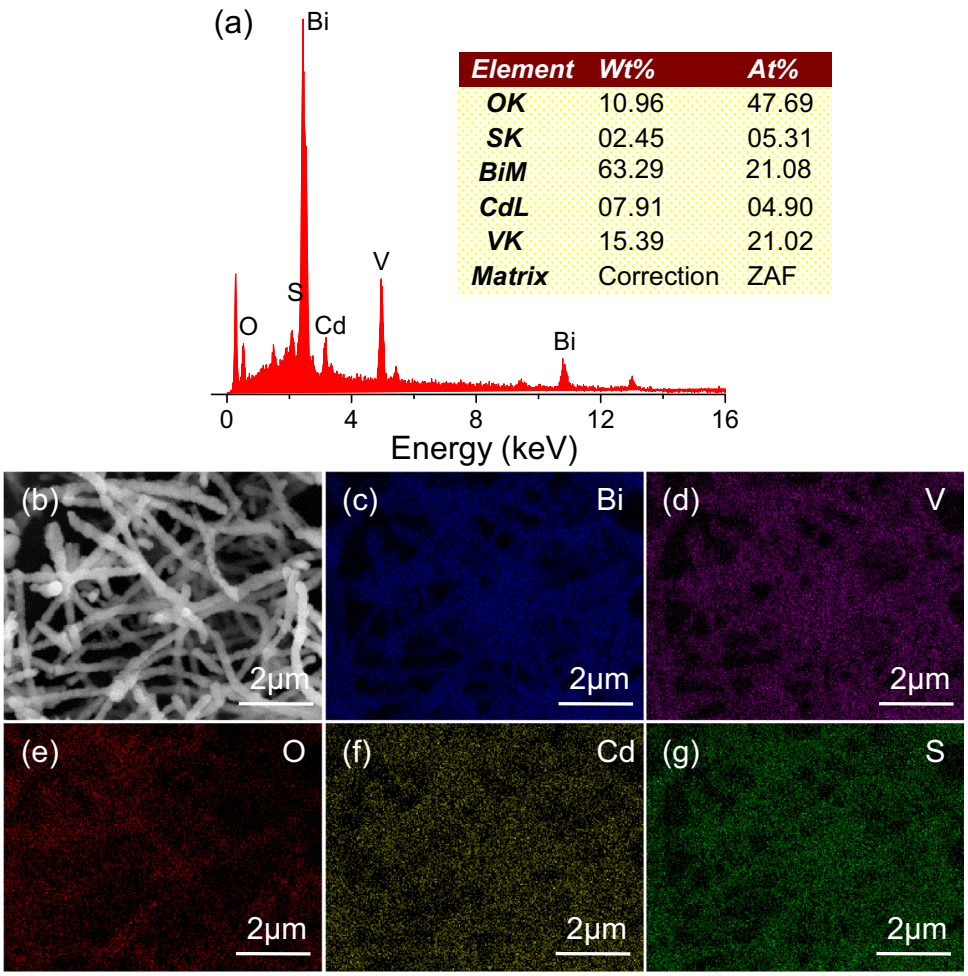

Fig. 4 EDS pattern (**a**) and elemental mapping (**b**–**g**) of the BVO/CdS-2

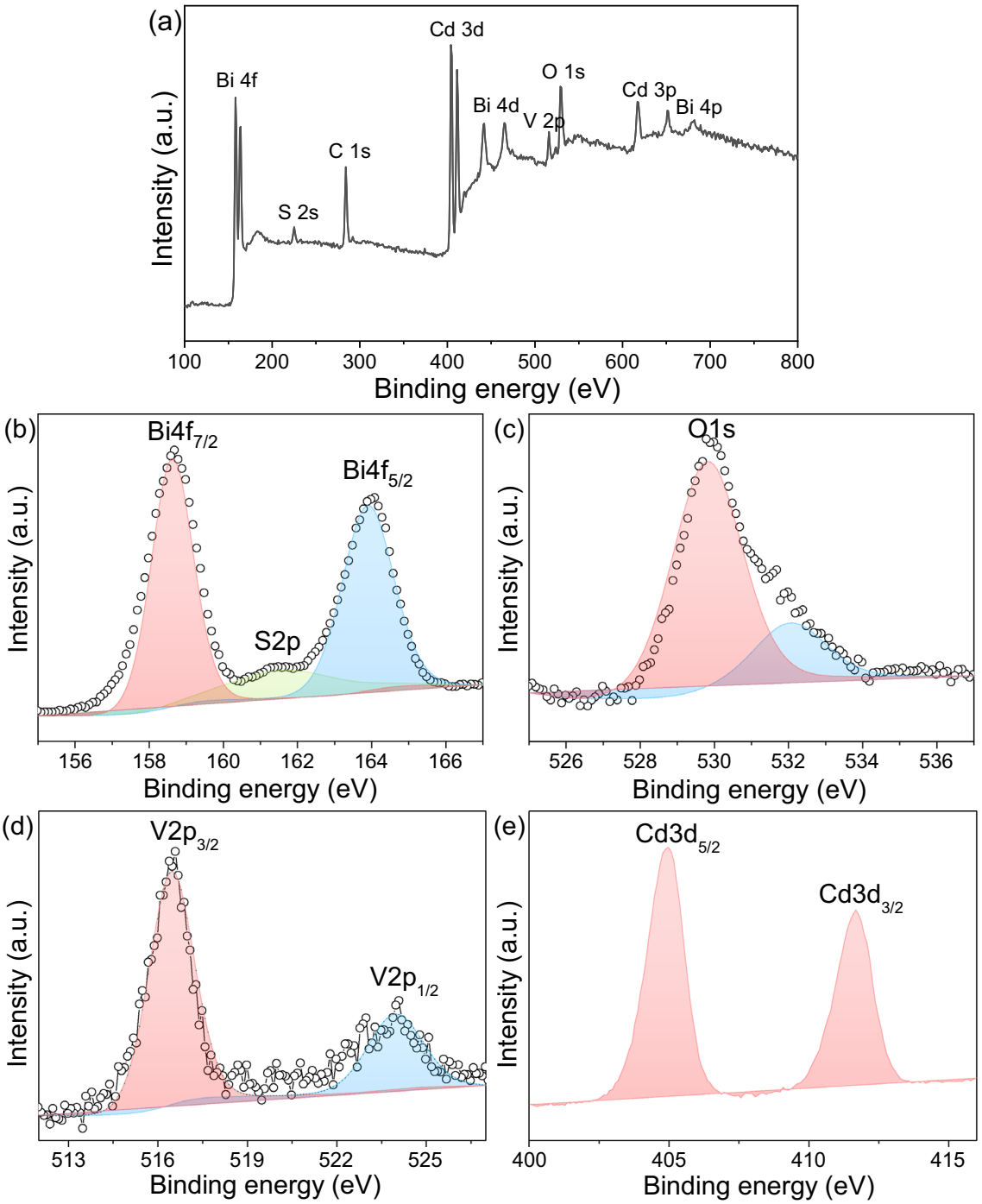

Fig. 5 Overall (**a**) and high resolution XPS spectrum of Bi 4f and S 2p (**b**), O 1 s (**c**), V 2p (**d**) and Cd 3d (**e**)

orbitals, respectively. The Cd 3d spectrum can be deconvoluted into two individual peaks at 405.7 and 412.4 eV matched well with Cd $3d_{5/2}$ and Cd $3d_{3/2}$, respectively, which is characteristic of Cd^{2+} in CdS (Fig. 5e) [20].

3.2 UV–vis absorption of $BiVO_4$/CdS nanofibers

The optical absorption and energy band structure as key factors for photocatalytic activity of semiconductor were evaluated by typical UV–vis diffuse reflection spectra. Both $BiVO_4$ and BVO/CdS-2

exhibit absorption in visible light regions (Fig. 6a). Nevertheless, the absorbance edge of $BiVO_4$ nanofibers (525 nm) is significantly expanded to visible light region for the BVO/CdS-2 composites (560 nm). The conspicuous red-shift of BVO/CdS-2 absorption could be ascribed to narrow bandgap of CdS, which would be beneficial to enhance the photocatalytic activity. The bandgap energy of $BiVO_4$ and BVO/CdS-2 can be estimated from a plot of $(\alpha hv)^2$ versus energy (hv) by intercepting the tangent to the x axis [22, 42]. As illustrated in Fig. 6b, the as-calculated bandgap value of the $BiVO_4$ nanofibers is about 2.46 eV, which is slightly higher than that of the BVO/CdS-2 (2.41 eV). The decoration of CdS nanoparticles on $BiVO_4$ nanofibers results in a decrease of the bandgap energy.

3.3 Specific surface areas of $BiVO_4$/CdS nanofibers

The specific surface areas of obtained samples were measured by using nitrogen adsorption and desorption isotherms. As exhibited in Fig. 7, the specific surface area of $BiVO_4$ and BVO/CdS-2 calculated by Brunauer–Emmett–Teller (BET) method are 2.51 and 6.53 $m^2\ g^{-1}$, respectively. The relatively high value of BVO/CdS-2 should be ascribed to the loaded CdS nanoparticles. Therefore, BVO/CdS-2 nanofibers would provide more active sites for the adsorption of dye molecules and photocatalytic reaction owing to enhanced surface area, and hence promote the photocatalytic activity of the composite. Furthermore, in comparison with the $BiVO_4$/CdS hybrid nanofibers synthesized by electrostatic interaction in our previous work (4.25 $m^2\ g^{-1}$) [40], BVO/CdS-2 heterojunctions obtained by hydrothermal method in this work show much larger specific surface area, which is probably due to the much rougher surface illustrated by the TEM images in Fig. 3e.

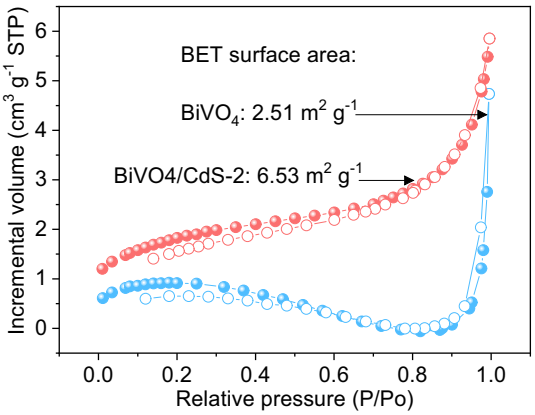

Fig. 7 N_2 adsorption–desorption isotherms of $BiVO_4$ and BVO/CdS-2 samples

3.4 Photocatalytic performance and mechanism of $BiVO_4$/CdS nanofibers

To assess and compare the photocatalytic activity of the samples, a series of experiments to photodegrade RhB aqueous were tested under visible light irradiation. Evolutions of the UV–vis spectral of RhB with the addition of $BiVO_4$ nanofiber and BVO/CdS composites are presented in Fig. 8. $BiVO_4$ nanofibers show negligible photodegradation of RhB after 3 h irradiation (Fig. 8a). Comparatively, a dramatical decrease of the absorption is achieved within the same time for BVO/CdS-2 sample, replying the enhanced photocatalytic performance. The blue-shift of the maximum absorption to short wavelength is because of dye's deethylation. Furthermore, the degradataion efficiency of all the samples were calculated according to a calibration curve of RhB

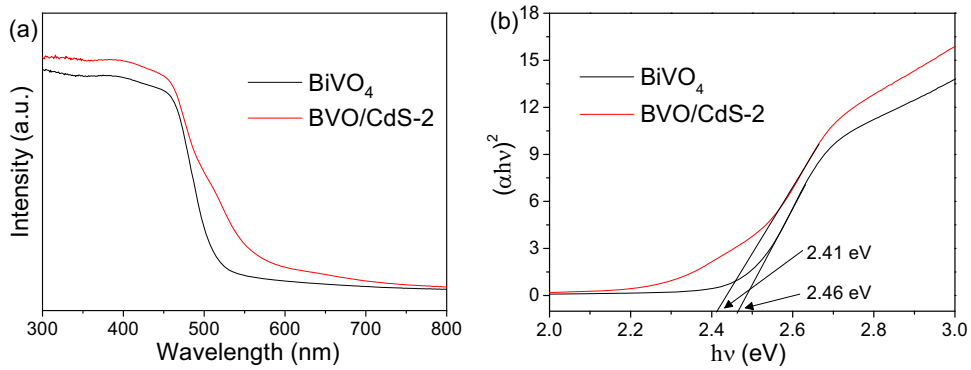

Fig. 6 UV–Vis DR spectra (**a**) and plot of $(\alpha hv)^2$ versus band gap energy (hv) (**b**) of $BiVO_4$ and BVO/CdS-2

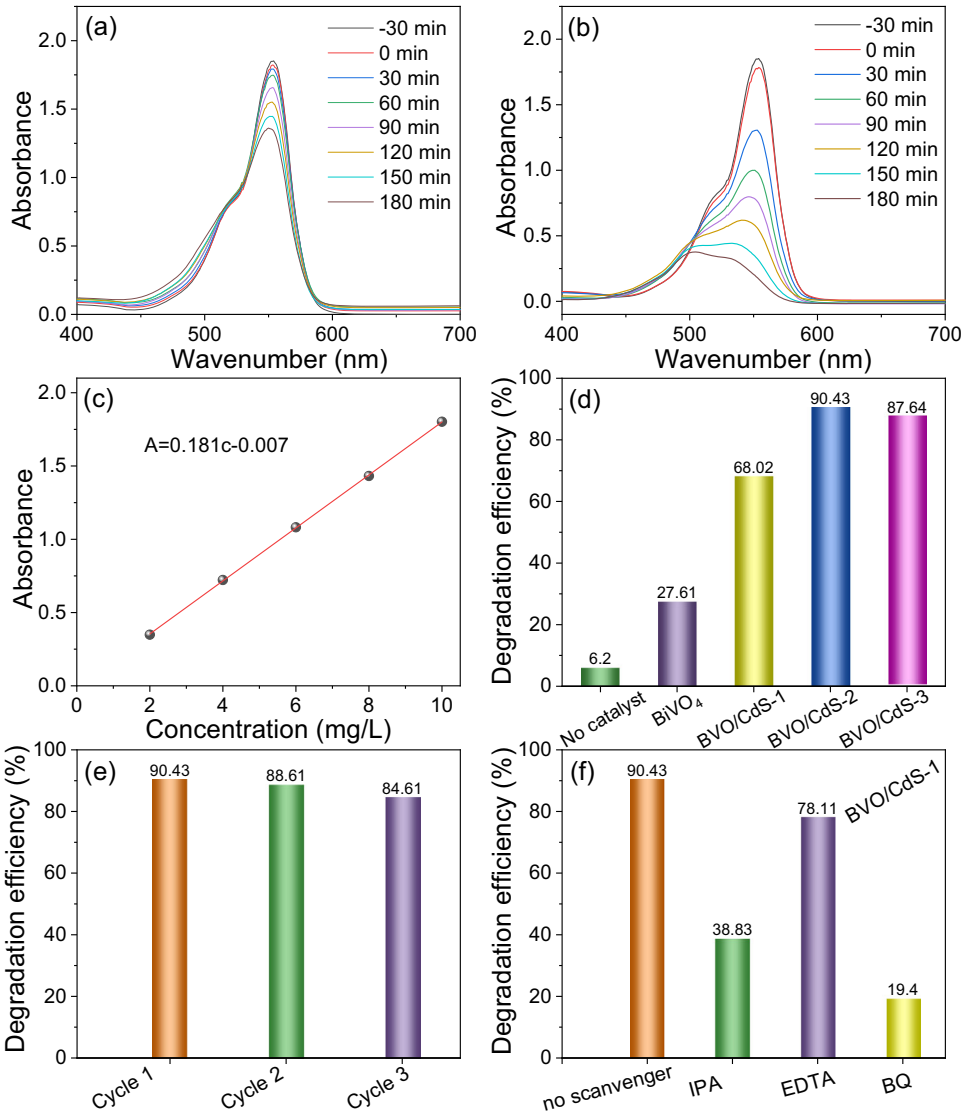

Fig. 8 UV–Vis spectral changes of RhB degraded by the $BiVO_4$ (**a**) and BVO/CdS-2 (**b**); photodegradation efficiency of RhB in the presence of various catalysts under visible light irradiation (**c**); RhB curves of ln(Co/C) versus irradiation time for different catalysts (**d**); The repeated photocatalytic degradation of RhB over BVO/CdS-2 nanofibers (**e**); photodegradation efficiency of RhB in the presence of various scavengers (**f**)

solution (Fig. 8c), and the results are shown in Fig. 8d. It can be noted that the degradation efficiency of no catalyst, $BiVO_4$, BVO/CdS-1, BVO/CdS-2 and BVO/CdS-3 nanofibers are 6.2%, 27.61%, 68.02%, 90.43% and 87.64% within 3 h under visible light irradiation, respectively. Evidently, the BVO/CdS composites show greatly increased photocatalytic performance after loading of CdS nanoparticles, and BVO/CdS-2 exhibits the highest removal efficiency. The photocatalytic performance increases along with the more deposition of CdS nanoparticles. However, too much CdS will result in the decrease of photocatalytic performance, which might be due to the low charge transfer separation efficiency on the semiconductor interface caused by thick CdS shells. These results are accordance with the SEM micromorphology and similar with our previous research work.

Maintaining the high photocatalytic efficiency for long-term use is an essential issue for photocatalysts in practical application. RhB photodegradation was repeated for three times to test the recyclability of BVO/CdS-2 nanofibers and each experiment was carried out under identical conditions. As shown in Fig. 8e, the photocatalytic activity of BVO/CdS-2 nanofiber did not show a significant loss after three cycles, indicating the good stability of the sample. To determine the important roles of reactive species in RhB photodegradation, Fig. 8f shows the RhB photocatalytic degradation efficiency with BVO/CdS-2 by introducing different capture agents of EDTA-2Na, BQ and IPA, corresponding to the removement

Table 1 Comparation of the increased ratio (R) of the photocatalytic efficiency of the BVO/CdS and other samples in literature

Sample	Light	Dyes	Irradiation time (min)	Degradation efficiency (%)	R	Ref
CdS QDs/npg-C_3N_4	Visible	RhB	90	88.2	1.85	[43]
CdS/$BiVO_4$	Visible	RhB	60	94.7	4.71	[27]
$BiVO_4$/CdS	Visible	RhB	120	85	5.31	[40]
$Mn_xZn_{1-x}Fe_2O_4$/C/CdS	Visible	RhB	140	97.8	1.30	[44]
CdS/BiOBr	Visible	RhB	60	97	2.49	[45]
BiOBr/CdS	Visible	RhB	40	90	2.26	[46]
$BiVO_4$/CdS	Visible	RhB	180	90.77	3.28	This work

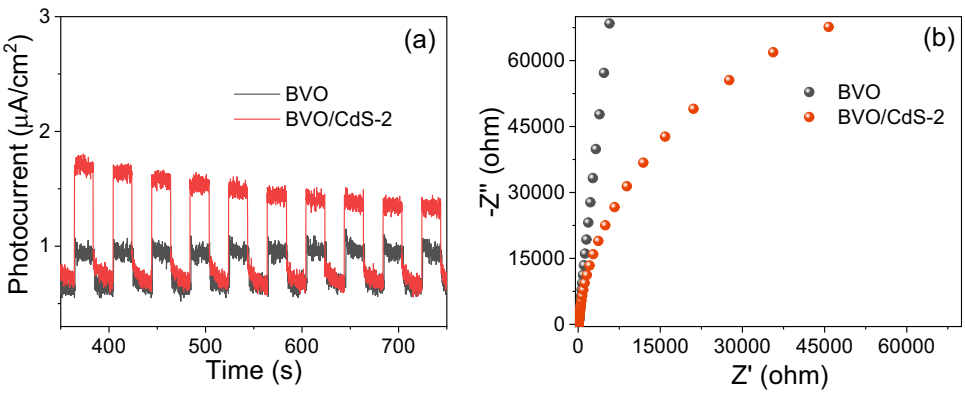

Fig. 9 Transient photocurrent responses (**a**) and EIS Nyquist plots (**b**) of electrodes of $BiVO_4$ and BVO/CdS-2 nanofibers

of active holes (h^+), superoxide radicals ($.O_2^-$) and hydroxyl radicals (.OH) reactive species, respectively. The photodegradation efficiency of RhB solution is obviously inhibited with the addition of BQ, IPA and EDTA, suggesting the involvement of $.O_2^-$, .OH and h^+ in the degradation of RhB. The results confirm that all the h^+, $.O_2^-$ and .OH act as the main active species in the photocatalytic process in the order of $.OH > .O_2 > h^+$.

Considering the differences of the composition, photocatalytic conditions by different researchers, we also compare the photocatalytic performance and improved ratio of the BVO/CdS-2 photocatalysts hydrothermal synthesized in this work with some other CdS-contained composites (Table 1). Paticullarly compared with our previous BVO/CdS [40], the BVO/CdS heterojunctions obtained by hydrothermal method show much larger specific surface area and CdS particle size, but lower photocatalytic efficiency than that of BVO/CdS heterojunctions prepared by electrostatic interaction. So, it seems that the particle size plays more important role to boost the photocatalytic activity of $BiVO_4$. Besides, a 3.28-time increase of degradation efficiency from $BiVO_4$ to BVO/CdS-2 was achieved, which is relativly higher than other CdS-contained composites in the literature.

The interfacial charge transfer of $BiVO_4$ and BVO/CdS-2 were measured by photocurrent transient response measurements with light on and off cycles under intermittent irradiation (Fig. 9a). In comparison with pure $BiVO_4$, the immobilization of CdS nanoparticles can enhance the reproducible photocurrent density, resulting in increase of the visible light photocatalytic activity and charge separation of BVO/CdS nanofibers. Furthermore, the photoelectrochemical characterization of surface-coated electrodes was also investigated by electrochemical impedance spectroscopy (EIS). As can be found in Fig. 9b, a smaller semicircle radius implies that BVO/CdS-2 nanofibers possess higher separation efficiency of photo-induced carries, which is in accordance with the larger photocurrent response of BVO/CdS-2 nanofibers.

On the basis of the above experimental results and previous reports, a proposed mechanism of visible light-induced photodegradation of RhB happened on BVO/CdS is schematically shown in Fig. 10. The

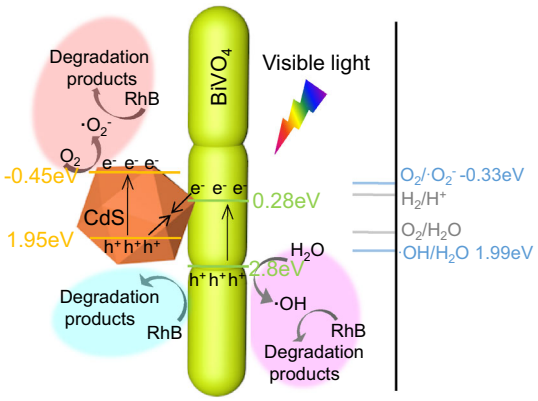

Fig. 10 Schematic diagram of the proposed photocatalytic mechanism

value band of $BiVO_4$ is more positive than the redox potential of .OH/H_2O (+ 1.99 eV) [47] and the conduction band (CB) of CdS is more negative than the standard redox potentials of $O_2/.O_2^-$ (− 0.33 eV) [48]. Upon irradiation with visible light, the photo-generated electrons in the CB of CdS are trapped by dissolved oxygen molecules to yield superoxide radical anions ($.O_2^-$), which should respond for the degradation of RhB. In addition, the .OH radicals achieved by the reaction of hole with surface-bound H_2O have strong oxidization ability for decomposing the RhB. Meanwhile, the photo-generated holes can also directly decompose the RhB to products.

4 Conclusions

In summary, fibrous $BiVO_4$/CdS heterojunctions were synthesized by using simple electrospinning and hydrothermal methods. The decoration of around 40 nm CdS nanoparticles furnishes the caterpillar shaped $BiVO_4$ nanofibers coarse surface with a specific area of 6.53 $m^2\ g^{-1}$, accompanied with apparently boosted visible light photodegradation ability and charge separation efficiency. Under the irradiation of visible light, the optimized $BiVO_4$/CdS-2 sample presents the highest photocatalytic efficiency as high as 91% mainly via the active species of $.O_2^-$ and .OH. Our results presented herein provide new insights into the rational design of nanostructured $BiVO_4$/CdS photocatalysts toward efficient, stable and sustainable visible light photodegradation application.

Acknowledgements

This work was supported by the Science and Technology Department of Shaanxi Province (2021JM-386), Provincial Joint Fund of Shaanxi (2021JLM-28) and Outstanding Youth Science Fund of Xi'an University of Science and Technology (2019YQ2-06), Priority Research and Development Foundations of Shaanxi Provincial Government (2021GY-215).

References

1. S. Chen, T. Takata, K. Domen, Particulate photocatalysts for overall water splitting. Nat. Rev. Mater. **2**, 17050–17067 (2017)
2. T. Hisatomi, K. Domen, Reaction systems for solar hydrogen production via water splitting with particulate semiconductor photocatalysts. Nat. Catal. **2**, 387–399 (2019)
3. T.W. Kim, K.S. Choi, Nanoporous $BiVO_4$ photoanodes with dual-layer oxygen evolution catalysts for solar water splitting. Science **343**, 990–994 (2014)
4. A. Malathia, J. Madhavan, M. Ashokkumarb, P. Arunachalamc, A review on $BiVO_4$ photocatalyst: activity enhancement methods for solar photocatalytic applications. Appl. Catal. A **555**, 47–74 (2018)
5. L.-G. Peng, H. Wang, J. Liu, M. Sun, F.-R. Ni, M.-J. Chang, H.-L. Du, J. Yang, Fabrication of fibrous $BiVO_4/Bi_2S_3/MoS_2$ heterojunction and synergetic enhancement of photocatalytic activity towards pollutant degradation. J. Solid State Chem. **299**, 122195 (2021)
6. B. Baral, D.P. Sahoo, K. Parida, Discriminatory {040}-reduction facet/Ag(0) schottky barrier coupled {040/110}-$BiVO_4$@Ag@CoAl-LDH Z-scheme isotype heterostructure. Inorg. Chem. **60**, 1698–1715 (2021)
7. B. Xiong, Y. Wu, J. Du, J. Li, B. Liu, G. Ke, H. He, Y. Zhou, $Cu_3Mo_2O_9/BiVO_4$ heterojunction films with integrated thermodynamic and kinetic advantages for solar water oxidation. ACS Sustain. Chem. Eng. **8**, 14082–14090 (2020)
8. Q. Xie, W. He, S. Liu, C. Li, J. Zhang, P.K. Wong, Bifunctional S-scheme g-C_3N_4/Bi/$BiVO_4$ hybrid photocatalysts toward artificial carbon cycling. Chin. J. Catal. **41**, 140–153 (2020)
9. Y. Wang, K. Ding, R. Xu, D. Yu, W. Wang, P. Gao, B. Liu, Fabrication of $BiVO_4/BiPO_4$/GO composite photocatalytic material for the visible light-driven degradation. J. Clean. Prod. **247**, 119108 (2020)
10. R. Han, M.A. Melo, Z. Zhao, Z. Wu, F.E. Osterloh, Light intensity dependence of photochemical charge separation in the $BiVO_4$/Ru-$SrTiO_3$: Rh direct contact tandem

photocatalyst for overall water splitting. J. Phys. Chem. C **124**, 9724–9733 (2020)
11. W. Zhao, J. Li, B. Dai, Z. Cheng, J. Xu, K. Ma, L. Zhang, N. Sheng, G. Mao, H. Wu, K. Wei, D.Y.C. Leung, Simultaneous removal of tetracycline and Cr(VI) by a novel three-dimensional AgI/$BiVO_4$ p-n junction photocatalyst and insight into the photocatalytic mechanism. Chem. Eng. J. **369**, 716–725 (2019)
12. G.C. Zhang, J. Zhong, M. Xu, Y. Yang, Y. Li, Z. Fang, S. Tang, D. Yuan, B. Wen, J. Gu, Ternary $BiVO_4$/NiS/Au nanocomposites with efficient charge separations for enhanced visible light photocatalytic performance. Chem. Eng. J. **375**, 122093 (2019)
13. C. Lai, M. Zhang, B. Li, D. Huang, G. Zeng, L. Qin, X. Liu, H. Yi, M. Cheng, L. Li, Z. Chen, L. Chen, Fabrication of CuS/$BiVO_4$ (0 4 0) binary heterojunction photocatalysts with enhanced photocatalytic activity for Ciprofloxacin degradation and mechanism insight. Chem. Eng. J. **358**, 891–902 (2019)
14. S. Xu, D. Fu, K. Song, L. Wang, Z. Yang, W. Yang, H. Hou, One-dimensional WO_3/$BiVO_4$ heterojunction photoanodes for efficient photoelectrochemical water splitting. Chem. Eng. J. **349**, 368–375 (2018)
15. B. Wang, W. Feng, L. Zhang, Y. Zhang, X. Huang, Z. Fang, P. Liu, In situ construction of a novel Bi/CdS nanocomposite with enhanced visible light photocatalytic performance. Appl. Catal. B **206**, 510–519 (2017)
16. J. Ran, J. Zhang, J. Yu, M. Jaroniec, S.Z. Qiao, Earth-abundant cocatalysts for semiconductor-based photocatalytic water splitting. Chem. Soc. Rev. **43**, 7787–7812 (2014)
17. A.B. Wong, S. Brittman, Y. Yu, N.P. Dasgupta, P. Yang, Core-shell CdS-Cu_2S nanorod array solar cells. Nano Lett. **15**, 4096–4101 (2015)
18. S. Sharma, S. Singh, N. Khare, Synthesis of polyaniline/CdS (nanoflowers and nanorods) nanocomposites: a comparative study towards enhanced photocatalytic activity for degradation of organic dye. Colloid Polym. Sci. **294**, 917–926 (2016)
19. F. Ye, H. Li, H. Yu, S. Chen, X. Quan, Constructing $BiVO_4$-Au@CdS photocatalyst with energic charge-carrier-separation capacity derived from facet induction and Z-scheme bridge for degradation of organic pollutants. Appl. Catal. B **227**, 258–265 (2018)
20. N. Clament Sagaya Selvam, Y.G. Kim, D.J. Kim, W.H. Hong, W. Kim, S.H. Park, W.K. Jo, Reduced graphene oxide-mediated Z-scheme $BiVO_4$/CdS nanocomposites for boosted photocatalytic decomposition of harmful organic pollutants. Sci. Total Environ. **635**, 741–749 (2018)
21. X. Wu, J. Zhao, L. Wang, M. Han, M. Zhang, H. Wang, H. Huang, Y. Liu, Z. Kang, Carbon dots as solid-state electron mediator for $BiVO_4$/CDs/CdS Z-scheme photocatalyst working under visible light. Appl. Catal. B **206**, 501–509 (2017)
22. Q. Li, Z. Guan, D. Wu, X. Zhao, S. Bao, B. Tian, J. Zhang, Z-Scheme BiOCl-Au-CdS heterostructure with enhanced sunlight driven photocatalytic activity in degrading water dyes and antibiotics. ACS Sustain. Chem. Eng. **5**, 6958–6968 (2017)
23. S. Bao, Q. Wu, S. Chang, B. Tian, J. Zhang, Z-scheme CdS-Au-$BiVO_4$ with enhanced photocatalytic activity for organic contaminant decomposition. Catal. Sci. Technol. **7**, 124–133 (2017)
24. L. Zou, H. Wang, X. Wang, High efficient photodegradation and photocatalytic hydrogen production of CdS/$BiVO_4$ heterostructure through Z-Scheme process. ACS Sustain. Chem. Eng. **5**, 303–309 (2016)
25. B. Han, S. Liu, Y.-J. Xu, Z.-R. Tang, 1D CdS nanowires-2D $BiVO_4$ nanosheets heterostructures toward photocatalytic selective fine-chemical synthesis. RSC Adv. **5**, 16476–16483 (2015)
26. W. Wang, Z.D. Hood, X. Zhang, I.N. Ivanov, Z. Bao, T. Su, M. Jin, L. Bai, X. Wang, R. Zhang, Z. Wu, Construction of 2D $BiVO_4$-CdS-Ti_3C_2Tx heterostructures for enhanced photo-redox activities. ChemCatChem **12**, 3496–3503 (2020)
27. Y. Lin, D. Pan, H. Luo, Hollow direct Z-Scheme CdS/$BiVO_4$ composite with boosted photocatalytic performance for RhB degradation and hydrogen production. Mater. Sci. Semicond. Process. **121**, 105453 (2021)
28. R. Guo, A. Yan, J. Xu, B. Xu, T. Li, X. Liu, T. Yi, S. Luo, Effects of morphology on the visible-light-driven photocatalytic and bactericidal properties of $BiVO_4$/CdS heterojunctions: a discussion on photocatalysis mechanism. J. Alloys Compd. **817**, 153246 (2020)
29. H. Yang, J. Fan, C. Zhou, Y. Wan, J. Zhang, J. Chen, G. Wang, R. Wang, C. Jiang, A Z-scheme $BiVO_4$/CdS hollow sphere with a high photocatalytic hydrogen evolution activity. Mater. Lett. **280**, 128317 (2020)
30. M.-J. Chang, W.-N. Cui, J. Liu, K. Wang, H.-L. Du, L. Qiu, S.-M. Fan, Z.-M. Luo, Construction of novel TiO_2/$Bi_4Ti_3O_{12}$/MoS_2 core/shell nanofibers for enhanced visible light photocatalysis. J. Mater. Sci. Technol. **36**, 97–105 (2020)
31. J. Liu, Q. Hui, M.-J. Chang, W.-N. Cui, T. Xi, L.-D. Wang, M. Sun, B. Yuan, F.-R. Ni, Facile fabrication of fibrous $Bi_4Ti_3O_{12}$/Bi_2S_3/MoS_2 with enhanced photocatalytic activities towards pollutant degradation under visible light irradiation. J. Mater. Sci.: Mater. Electron. **31**, 17688–17702 (2020)
32. M. Yu, C. Shang, G. Ma, Q. Meng, Z. Chen, M. Jin, L. Shui, Y. Zhang, Z. Zhang, M. Yuan, X. Wang, G. Zhou, Synthesis and characterization of mesoporous $BiVO_4$ nanofibers with enhanced photocatalytic water oxidation performance. Appl. Surf. Sci. **481**, 255–261 (2019)

33. H. Liu, W. Yang, L. Wang, H. Hou, F. Gao, Electrospun $BiVO_4$ nanobelts with tailored structures and their enhanced photocatalytic/photoelectrocatalytic activities. CrystEngComm **19**, 6252–6258 (2017)
34. M.J. Nalbandian, M. Zhang, J. Sanchez, Y.-H. Choa, D.M. Cwiertny, N.V. Myung, Synthesis and optimization of $BiVO_4$ and co-catalyzed $BiVO_4$ nanofibers for visible light-activated photocatalytic degradation of aquatic micropollutants. J. Mol. Catal. A: Chem. **404–405**, 18–26 (2015)
35. C. Lv, J. Sun, G. Chen, Y. Zhou, D. Li, Z. Wang, B. Zhao, Organic salt induced electrospinning gradient effect: achievement of $BiVO_4$ nanotubes with promoted photocatalytic performance. Appl. Catal. B **208**, 14–21 (2017)
36. Z. Liu, Q. Lu, C. Wang, J. Liu, G. Liu, Preparation of bamboo-shaped $BiVO_4$ nanofibers by electrospinning method and the enhanced visible-light photocatalytic activity. J. Alloys Compd. **651**, 29–33 (2015)
37. M. Zhang, C. Shao, X. Li, P. Zhang, Y. Sun, C. Su, X. Zhang, J. Ren, Y. Liu, Carbon-modified $BiVO_4$ microtubes embedded with Ag nanoparticles have high photocatalytic activity under visible light. Nanoscale **4**, 7501–7508 (2012)
38. R.P. Antony, P.S. Bassi, F.F. Abdi, S.Y. Chiam, Y. Ren, J. Barber, J.S.C. Loo, L.H. Wong, Electrospun Mo-$BiVO_4$ for efficient photoelectrochemical water oxidation: direct evidence of improved hole diffusion length and charge separation. Electrochim. Acta **211**, 173–182 (2016)
39. H. Liu, H. Hou, F. Gao, X. Yao, W. Yang, Tailored fabrication of thoroughly mesoporous $BiVO_4$ nanofibers and their visible-light photocatalytic activities. ACS Appl. Mater. Interfaces. **8**, 1929–1936 (2016)
40. J. Liu, L. Qiu, M.-J. Chang, B. Yuan, M. Sun, S.-M. Fan, W.-N. Cui, Q. Hui, F.-R. Ni, M.-Y. Li, Y.-Q. Li, Z.-M. Luo, Fabrication of novel fibrous $BiVO_4$/CdS heterostructures by electrospinning method for efficient visible light photodegradation. Mater. Chem. Phys. **247**, 122858 (2020)
41. M.J. Chang, W.N. Cui, H. Wang, J. Liu, H.L. Li, H.L. Du, L.G. Peng, Recoverable magnetic $CoFe_2O_4$/BiOI nanofibers for efficient visible light photocatalysis. Colloids Surf. A **562**, 127–135 (2019)
42. H. Huang, Y. He, X. Du, P.K. Chu, Y. Zhang, A general and facile approach to heterostructured core/shell $BiVO_4$/BiOI p–n junction: room-temperature in situ assembly and highly boosted visible-light photocatalysis. ACS Sustain. Chem. Eng. **3**, 3262–3273 (2015)
43. Q. Fan, Y. Huang, C. Zhang, J. Liu, L. Piao, Y. Yu, S. Zuo, B. Li, Superior nanoporous graphitic carbon nitride photocatalyst coupled with CdS quantum dots for photodegradation of RhB. Catal. Today **264**, 250–256 (2016)
44. Y. Cheng, T. Wu, L. Xu, C. Liu, Z. Jiang, Q. Zhang, Y. Zou, Y. Chen, J. Li, X. Liu, A novel visible-light-driven ternary magnetic photocatalyst Mn Zn1-Fe_2O_4/C/CdS: fabrication, characterization and application. Mater. Chem. Phys. **262**, 124308 (2021)
45. W. Cui, W. An, L. Liu, J. Hu, Y. Liang, Synthesis of CdS/BiOBr composite and its enhanced photocatalytic degradation for Rhodamine B. Appl. Surf. Sci. **319**, 298–305 (2014)
46. J. You, L. Wang, W. Bao, A. Yan, R. Guo, Synthesis and visible-light photocatalytic properties of BiOBr/CdS nanomaterials. J. Mater. Sci. **56**, 6732–6744 (2021)
47. B. Luo, D. Xu, D. Li, G. Wu, M. Wu, W. Shi, M. Chen, Fabrication of a Ag/Bi_3TaO_7 plasmonic photocatalyst with enhanced photocatalytic activity for degradation of tetracycline. ACS Appl. Mater. Interfaces. **7**, 17061–17069 (2015)
48. F. Chen, Q. Yang, J. Sun, F. Yao, S. Wang, Y. Wang, X. Wang, X. Li, C. Niu, D. Wang, G. Zeng, Enhanced photocatalytic degradation of tetracycline by AgI/$BiVO_4$ heterojunction under visible-light irradiation: mineralization efficiency and mechanism. ACS Appl. Mater. Interfaces. **8**, 32887–32900 (2016)